Approximation of Range in Materials as a Function of Incident Electron Energy

Gregory Wilson and JR Dennison

***Abstract*— A simple composite analytic expression has been developed to approximate the electron range in materials. The expression is applicable over more than six orders of magnitude in energy (<10 eV to >10 MeV) and range (10^{-9} m to 10^{-2} m), with uncertainty of ≤20% for most conducting, semiconducting and insulating materials. This is accomplished by fitting data from two standard NIST databases [ESTAR for the higher energy range and the electron IMFP (inelastic mean free path) for the lower energies]. In turn, these data have been fit with well-established semi-empirical models for range and IMFP that are related to standard materials properties (*e.g.*, density, atomic number, atomic weight, stoichiometry, band gap energy). A single free parameter, the effective number of valence electrons per atom N_v, is used to predict the range over the entire energy span.**

***Index Terms*—range, inelastic mean free path, spacecraft charging**

I. Introduction

THE range, *R*, or maximum distance an electron of a given incident energy can penetrate through a material before all kinetic energy is lost and the electron comes to rest, is a common way to parameterize electron interactions with materials. The range is used in spacecraft charging calculations to predict the charge distribution of deposited electrons in materials and to model secondary and backscattered electron emission. It is also used to predict the distribution of energy deposited by incident electrons as they traverse a material; this distribution is further used to model radiation induced conductivity. It is therefore important for spacecraft charging models to have a realistic, reasonably accurate, and efficient expression to predict the approximate range of electron energies commonly encountered in space plasma fluxes, from ~10 eV to ~10 MeV. This expression needs to be readily implemented for a wide array of conducting, semiconducting and insulating spacecraft materials with a minimal number of fitting parameters.

Figure 1 offers dramatic visual evidence of the validity of the range of electrons in a material. The white line seen at the center of the side view results from melting of the plastic target during discharge, as electrons deposited in a narrow distribution at a depth of $R \approx 3$ mm by a monoenergetic ~1 MeV electron beam are released.

Research was supported by funding from the NASA James Webb Space Telescope Program through Goddard Space Flight Center and a Utah State University Undergraduate Research and Creative Opportunities grant.

Gregory Wilson is a senior physics major at Utah State University in Logan, UT 84322 USA (gregdwilson@gmail.com).

JR Dennison is a professor in the Physics Department at Utah State University in Logan, UT 84322 USA (phone: 435-797-2936; fax: 435-797-2492; e-mail: JR.Dennison@usu.edu).

II. Theory

The desired range expression can be developed by merging well known semi-empirical models for the interaction of electrons with materials in different energy regimes by employing the continuous-slowing-down approximation (CSDA). In the CSDA, the rate of energy loss (or total stopping power) at every position along the penetration path, $\frac{dE}{dz}$, is assumed constant; variations in energy-loss rate with energy, *E*, or penetration depth, *z*, are neglected. For a given incident energy, E_b, the CSDA range is obtained by integrating the reciprocal of the total stopping power with respect to energy over the full penetration depth such that $E_b = \int_0^R \frac{dE}{dz} dz$ [1, 2].

For a constant energy-loss rate in the CSDA, $\frac{dE}{dz} = {E_b}/{R} = {E_m}/{\lambda_m} = {E_{mim}}/{\lambda_{min}}$ is a constant. Here E_m is equal to mean energy lost per collision occurring at mean free path $\lambda_m \equiv \lambda_{IMFP}(E_m)$, and E_{mim} is the energy at the minimum in the inelastic mean free path curve at $\lambda_{min} \equiv \lambda_{IMFP}(E_{min})$. A reasonable approximation for E_m is the geometric mean of the plasmon energy and the bandgap energy, E_g, times an empirically determined factor of 2.8 [3]

$$E_m = 2.8\left[(E_p)^2 + (E_{gap})^2\right]^{1/2}$$

where the plasmon energy is

$$E_p = \hbar(N_V {q_e}^2/m_e\varepsilon_0)^{1/2}$$

N_v, is the effective number of valence electrons per atom, $\hbar$ is Planck's constant divided by 2π, ε_0 is the permittivity of free space, and q_e and m_e are the electron charge and rest mass, respectively.

Tabulated values of the electron ranges at high energies using the CSDA can be found in the NIST ESTAR database spanning incident energies from E_{HI}~20 keV up to ~1 GeV [4]. The CSDA can also be applied to lower energy ranges. The NIST electron inelastic mean free path (IMFP) database [5] has tabulated values for the IMFP, which is closely related to the range as shown below, which are valid for energies from ~30 eV to E_{LO}~1 keV. Thus, in order to create an

Figure 1. Front (Left) and side (Right) views of a Lichtenberg discharge tree. The white line (Right)indicates the narrow distribution of deposited charge from a ~1 MeV electron beam at R≈3 mm.

analytic expression for the full range of energies desired, the problem can be broken into three parts according to energy of the incident electron: a high energy range for $E_b>E_{LO}\equiv 1$ keV; a mid-energy range for $E_m<E_b<E_{LO}$; and a low energy range for energies $E_b<E_m$.

A. High Energy Range

A simple power law approximation for the range is used

$$R_{HE}(E) = bE^n \left\{1 + \frac{E/N_V}{m_e c^2}\right\}$$

where the term in brackets is a first order relativistic correction that becomes significant above ~10^5 eV. Figure 2 shows the fit to tabulated data for Au from the ESTAR database, using both a simple power law and a power law with the first order relativistic correction. Figure 3 shows fits to the Au data using several range approximation formulas.

The stopping power exponent n is determined by requiring that the expressions for $R_{HE}(E)$ matches the more accurate low energy (non-relativistic) Bethe-Joy range expression based on the Bethe stopping power formula [6] as extended by Tanuma [7] used in conjunction with the NIST ESTAR database [4] ,

$$R_{BJ}(E) = \frac{(4\pi\epsilon_0)^2 M_A}{2\pi {q_e}^2 Z_A \rho_m} \frac{E^2}{ln\left(\sqrt{\frac{e}{2}}\left[\frac{E/N_V}{E_m} + k\right]\right)}$$

at two energies E_{LO} and E_{HI}. Here M_A is the atomic weight, Z_A as the atomic number, ρ_m is the mass density, and k=0.8 is a fixed empirical constant. $E_{HI}\equiv 20$ keV is the lower energy at which data are available for all materials in the ESTAR database and $E_{LO}\equiv 1$ keV is the upper energy at which data are

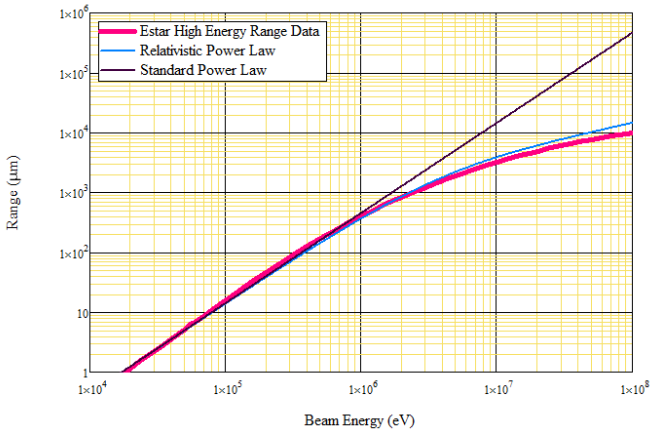

Figure 2. Comparison between the standard power law and the relativistic power law for Au. The relativistic power law allows approximations for energies up to 10 MeV with percent errors ~20%.

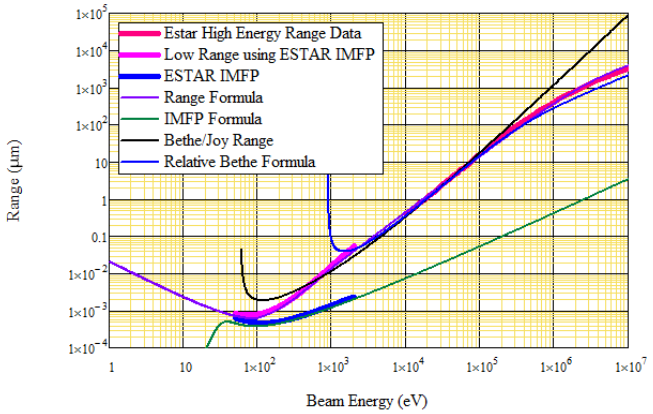

Figure 3. Comparison between several range approximations and the data from the ESTAR database for Au. The IMFP data for Au are also plotted along with the TPP-2M IMFP formula for $\lambda_{IMFP}(E)$.

available for all materials in the IMFP database. This leads to an expression for the stopping power exponent

$$n = ln\left[\frac{E_{LO}\, ln\left\{\sqrt{\frac{e}{2}}\left[\frac{E_{HI}/N_V}{E_m} + k\right]\right\}(2m_e c^2 N_V + E_{HI})(m_e c^2 N_V + E_{LO})^2}{E_{HI}\, ln\left\{\sqrt{\frac{e}{2}}\left[\frac{E_{LO}/N_V}{E_m} + k\right]\right\}(2m_e c^2 N_V + E_{LO})(m_e c^2 N_V + E_{HI})^2}\right] = \frac{}{ln[E_{LO}/E_{HI}]}$$

Note that the only free parameter in this expression is N_V, along with the electron mass and the fixed empirical constant k=0.8.

The high energy expression for $R_{HE}(E)$ is normalized to the mid-energy expression at E_{LO}, as detailed below, by setting

$$b = \frac{E_{LO}^{1-n}}{E_m\left(1 - exp\left[-\frac{E_{LO}}{E_m}\right]\right)\left\{1 - \left[1 + \left(\frac{E_{LO}/N_V}{E_m}\right)^2\right]^{-1}\right\}}$$

Again, note that the only free parameter in this expression is N_V, along with E_m which is expressed above in terms of N_V and the band gap energy, E_{gap}.

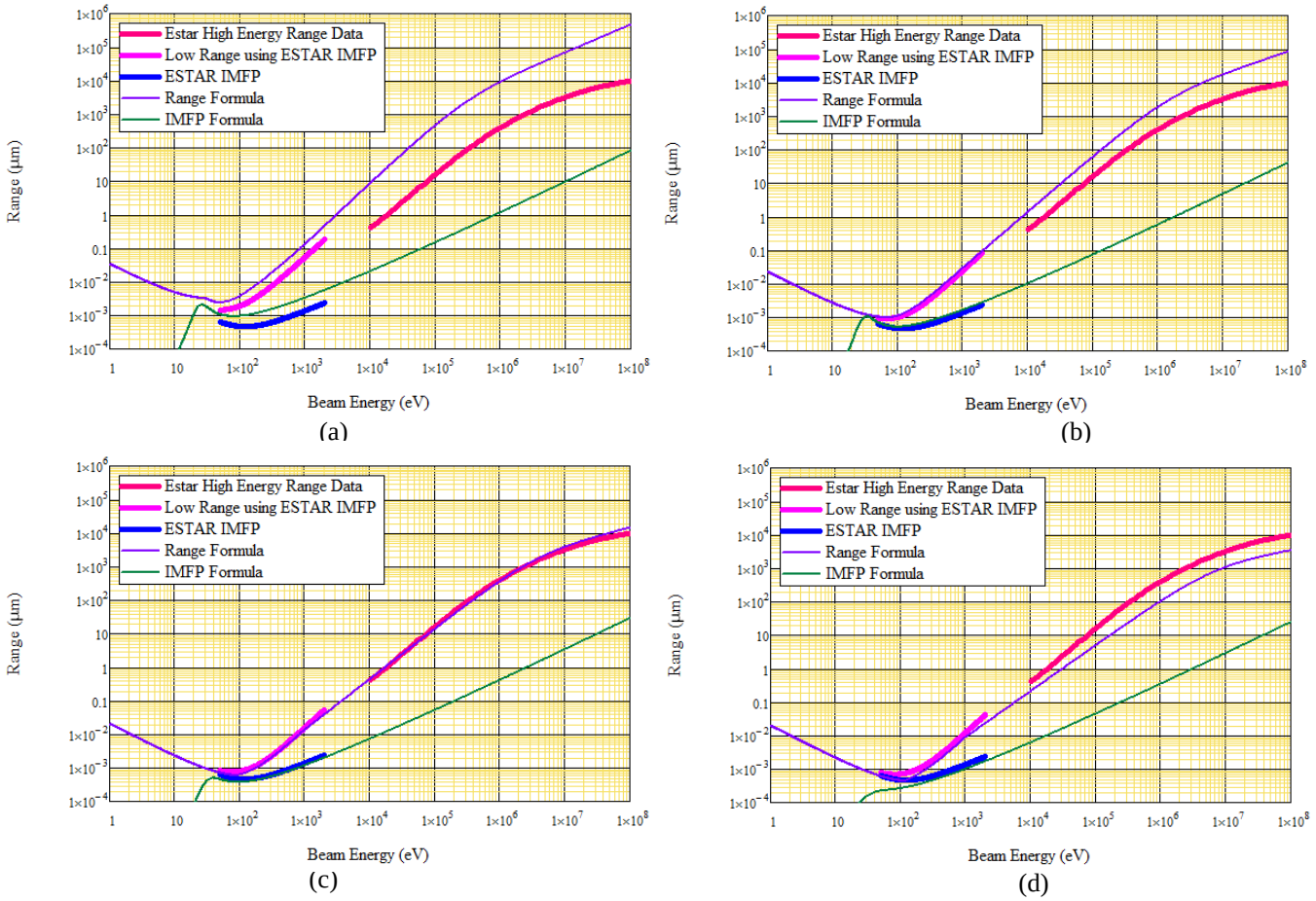

Figure 4. Graphs showing the variation of the range expression by changing the single fitting parameter N_v. For graphs (a) through (d), N_v = 1, 5, 12 (best fit) and 20, respectively.

B. Mid-Energy Range

Direct extrapolation of the range from the ESTAR data to lower energies is not valid for energies comparable to the atomic electronic structure, typically a few keV and below, because the discrete energy nature of the collisions becomes important. However, a simple extension of the CSDA to lower energies can relate the range to the electron IMFP, where

$$\frac{dE}{dz} = {E_b}/{R(E_b)} = \left[{E_m}/{\lambda_{IMFP}(E_b)}\right]\left(1 - e^{-E_b/E_m}\right)$$

Here the stopping power is again assumed equal to the total energy lost (incident energy, E_b) divided by the total distance traveled (range, R). This is set equal to the mean energy lost per collision, E_m, divided by the mean distance traveled per collision all times the probability that a collision occurs, $\left(1 - e^{-R/\lambda_m}\right)$=$\left(1 - e^{-E_b/E_m}\right)$. Here, the energy dependence in the range is fully contained in the energy dependence of the mean free path. For E_b>E_m, $\lambda_{IMFP}(E_b)$ is assumed to be given by the TPP-2M formula used in conjunction with the NIST IMFP database [5]:

$$\lambda_{IMFP}(E) = EE_p^{-2}[\beta ln(\gamma E) - CE^{-1} + DE^{-2}]^{-1}$$

where

$$\beta \equiv -0.1 + 0.34E_m^{-1} + 0.069\rho_m^{0.1}$$
$$\gamma \equiv 0.191\rho_m^{-\frac{1}{2}}$$
$$C \equiv 1.97 - 0.91U \text{ with } U \text{ in eV}$$
$$D \equiv 53.4 - 20.8U$$
$$U \equiv \frac{N_v\rho_m}{M_A}$$

Once again, by using the proposed equations of Tanuma contained in the TPP-2M model, the only free parameter in this expression is N_V, along with the materials constants E_{gap} (through E_m) plus M_A and ρ_m. Because of the shallow core levels (generally with binding energies <30 eV) that may contribute significant intensity to the energy-loss function, there arises an ambiguity in the choice of the value of the number of valence electrons [8]. While E_{gap} may be considered an additional fitting parameter for insulators, its effect on R is minimal causing primarily a small vertical shift in the range curve.

C. Low Energy Range

To calculate the range for E_b<E_m, we assume that the energy loss per collision of the low energy collisions is constant and equal to the mean excitation energy E_m, but that the probability that an electron undergoes one such inelastic collision falls off as $R/\lambda_m\left(e^{-R/\lambda_m}\right)$=$E_b/E_m\left(e^{-E_b/E_m}\right)$, while for E_b<E_m, the IMFP is constant and equal to the IMFP

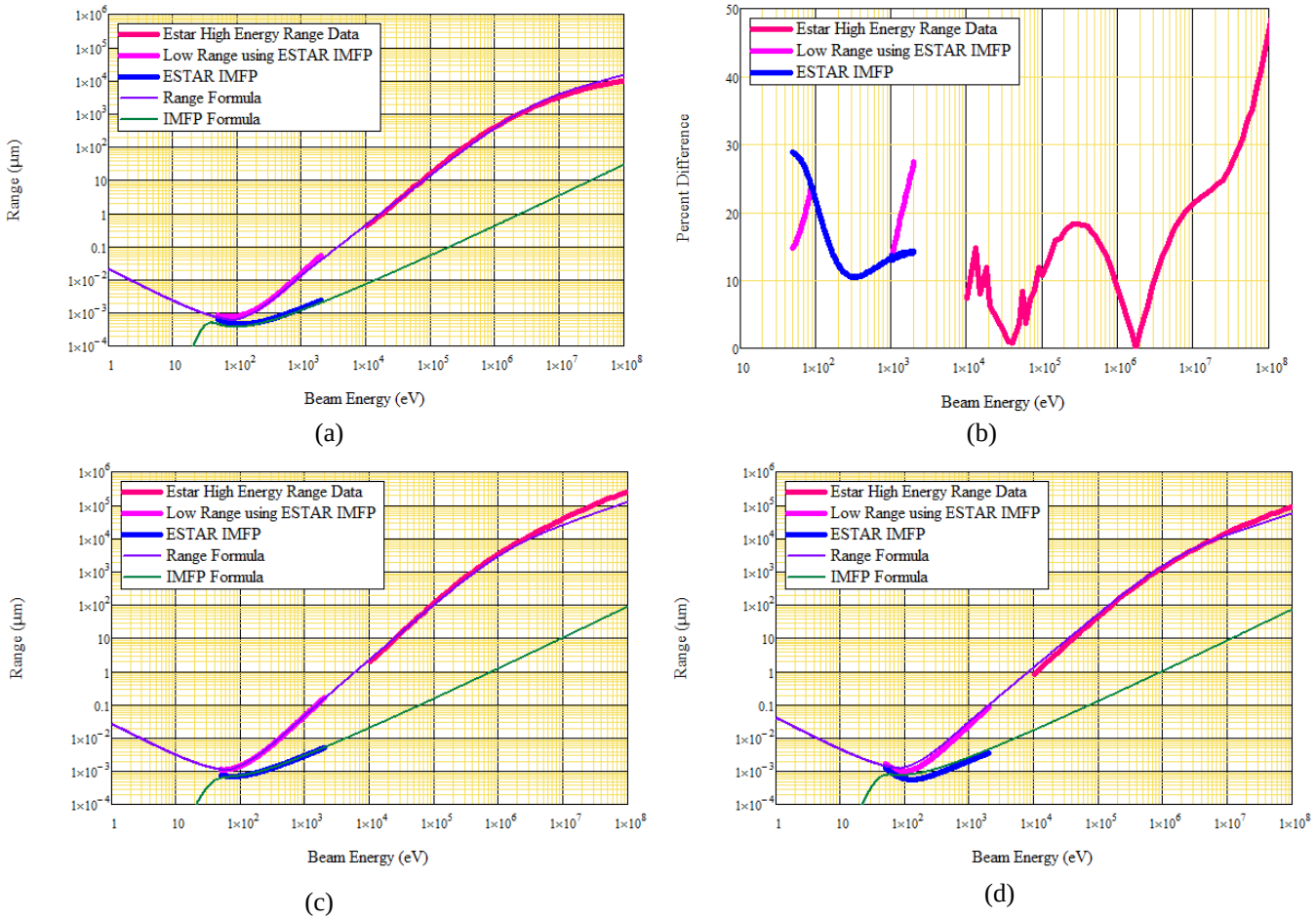

Fig. 5. (a) Comparison of the range formula for Au with N_v = 12.0 . (b) Residual plot of Au range data in Fig 5. (c) Comparison of the range formula for Kapton with N_v=4.1. (d) Comparison of the range formula for Al_2O_3 with N_v=5.0.

at the mean energy loss or $\lambda_{IMFP}(E_m)=\lambda_m$. This simple low energy approximation avoids the unusual asymptotic behavior exhibited by the TPP-2M expression at energies below E_m that is evident in the green curves in Fig. 4.

D. Composite Range Function

The final result is a continuous composite analytic approximation to the range with a single fitting parameter spanning from <10 eV to > 10 MeV:

$$R(E;N_V) = \begin{cases} \left[\frac{E}{E_m}\right] \frac{\lambda_{IMFP}(E_m)(1-exp[-1])}{\left(1-exp\left[-\frac{E}{E_m}\right]\right)^2} & ;E < E_m \\ \left[\frac{E}{E_m}\right] \frac{\lambda_{IMFP}(E)}{1-exp\left[-\frac{E}{E_m}\right]} & ;E_m \le E \le E_{HI} \\ bE^n\left(1-\left[1+\left[\frac{E/N_V}{m_e c^2}\right]\right]^{-2}\right) & ;E > E_{HI} \end{cases}$$

Figures 5(a), 5(c) and 5(d) show fits to data for three prototypical materials: the conductor Au; the polymeric insulator polyimide (Kapton), and the insulating ceramic Al_2O_3. Table I lists the fitting parameter N_V, along with materials properties and derived values, for 14 typical spacecraft materials. The residual curve for the fit for Au is shown in Fig. 5(b).

III. Applications

The usefulness of an analytical approximation of the range to spacecraft applications can easily be demonstrated by considering expressions for the dose rate and the radiation induced conductivity; both expressions require an energy dependent range expression.

The dose rate is defined as the energy deposited by incident radiation per unit mass. The dose rate in the CSDA for a homogeneous material is proportional to the volume in which radiation energy is deposited, which is equal to the beam cross section times R [9]. Thus,

$$\dot{D} \equiv \frac{\partial D}{\partial t} = \frac{E_o J_{in}}{\rho_m R q_e} \propto R^{-1}$$

The dose rate for Au as a function of incident energy is shown in Fig. 6.

Table I. Materials Properties and Fitting Parameters

Material Name	Material Formula	Fitting Parameter N_V	Material Properties ρ_m (gm/cm^3)	Z_A	M_A (amu)	E_{gap} (eV)	Derived Values n	b (μm/eV^n)	E_P (eV)	E_m (eV)	λ_{min} (nm)
Graphite	C	5.3	1.7	6	12.01	0.1	0.642	0.7143	24.87	69.6	0.793
Amorphous C	C	4.0	2.0	6	12.01	0.1	0.676	0.3877	23.43	65.6	0.614
Aluminum	Al	5.0	2.7	13	26.98	0.0	0.668	0.5075	20.31	56.9	0.467
Silicon	Si	5.0	2.33	14	28.09	1.11	0.676	0.5422	18.49	51.9	0.438
Copper	Cu	8.3	8.96	29	63.55	0.0	0.561	0.7821	31.06	87.0	0.422
Germanium	Ge	9.8	5.32	32	72.64	0.66	0.571	1.355	24.32	68.1	0.477
Silver	Ag	10.6	10.5	47	107.87	0.0	0.536	1.217	29.17	81.7	0.416
Gold	Au	12.0	19.32	79	196.97	0.0	0.508	1.261	31.15	87.2	0.371
Polyethylene	$[C_2H_4]_n$	2.5	0.94	2.65	4.64	2.9	0.727	0.2354	20.43	57.8	0.642
Polyimide	$[C_{22}H_{10}N_2O_5]_n$	4.1	1.42	5.01	9.769	2.3	0.678	0.4582	22.165	62.4	0.652
PTFE	$[C_2F_4]_n$	6.0	2.2	8.01	16.023	6	0.620	0.8794	26.06	78.9	0.865
Aluminum Oxide	Al_2O_3	5.0	3.97	10	30.392	9.9	0.628	0.5188	28.33	84.0	0.746
Silicon Dioxide	SiO_2	5.0	2.32	9.98	19.99	8.9	0.653	0.6215	21.87	66.1	0.711
Glass, Pyrex	doped SiO_2	6.2	2.32	9.98	19.99	4	0.626	0.8150	24.36	69.1	0.656

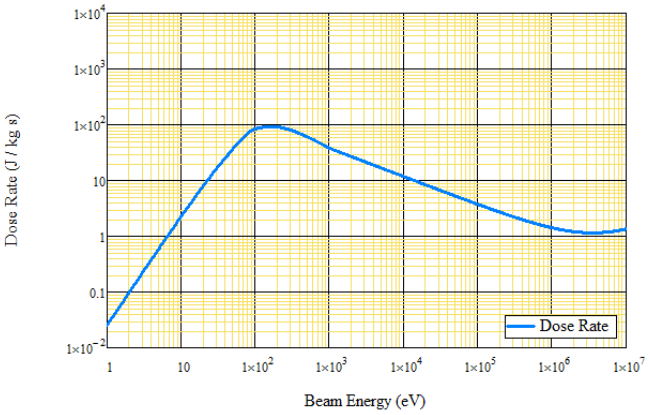

Figure 6. Dose rate as a function of energy in the CSDA for Au.

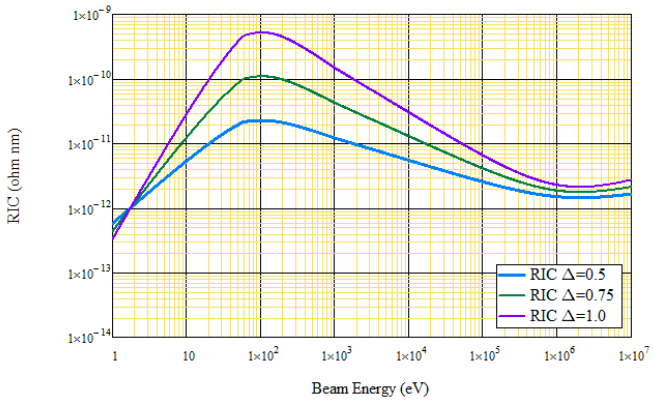

Figure 7. RIC as a function of energy in the CSDA for polyimide.

Radiation Induced Conductivity (RIC) is the enhanced conductivity that results from the energy deposited in this volume. In the CSDA

$$\sigma_{ric}(\dot{D}) = k_{ric}\dot{D}^{\Delta} \propto R^{-\Delta}$$

with ½<Δ<1 [10]. Figure 7 shows the RIC for Kapton as a function of incident energy for three values of Δ. Notice that both $\dot{D}$ and σ_{RIC} exhibit energy dependent maxima as a consequence of the minimum in the range expression.

Secondary electron (SE) emission is another extension of the range which would be highly beneficial. In the CSDA, the SE yield can be expressed as

$$\delta_{SE}(E, N_v, \delta_{max}, E_{max}) = \frac{\delta_{max}}{1 - exp[-R(E)/\lambda_{SE}]}\left\{1 - exp\left[-\frac{R(E)}{\lambda_{SE}}\left(\frac{E}{E_{max}}\right)^{\eta}\right]\right\}$$

Work is underway to develop an expression for the SE yield in terms of the range expression developed here. The expression would have three independent free parameters; N_V and the maximum SE yield δ_{max} at energy E_{max}.

References

1. Reimer, L., 2000, "Scanning Electron Microscopy: Physics of Image Formation and Microanalysis," Measurement Sci. Technol. 11, 1826.
2. Spencer, L., 1955, "Theory of Electron Penetration," Phys. Rev. 98, 1597.
3. Alig, R., and S. Bloom, 1975, "Electron-Hole-Pair Creation Energies in Semiconductors," Phys. Rev. Lett. 35, 1522.
4. National Institute of Standards and Technology, 2010, "ESTAR, Stopping Power and Range Tables for Electrons" (http://physics.nist.gov/PhysRefData/Star/Text/ESTAR.html).
5. National Institute of Standards and Technology, 2010, "NIST Electron Inelastic-Mean-Free-Path Database: Version 1.1," (http://www.nist.gov/data/nist71.htm).
6. Bethe, H., and W. Heitler, 1934, "On the Stopping of Fast Particles and on the Creation of Positive Electrons," in Proceedings of the Royal Society of London. Series A, Containing Papers of a Mathematical and Physical Character 146, 83.
7. Tanuma, S., C. Powell, and D. Penn, 2005, "Calculations of Stopping Powers of 100 eV to 30 keV Electrons in 10 Elemental Solids," Surf. Inter. Anal. 37, 978.
8. Tunuma, S, C.J. Powell and D.R. Penn, 1997, "Calculations of Electron Inelastic Mean Free Paths (IMFPs) VI. Analysis of the Gries Inelastic

Scattering Model and Predictive IMFP Equation," Surf. Inter. Anal. 25, 25.
9. Roth, J. A., R. Hoffmann, and J. Dennison, 2009, "Effects of Radiation Induced Conductivity on Electrostatic Discharge in Insulating Materials," in Proceedings of the 1st AIAA Atmospheric and Space Environments Conference (San Antonio, TX).
10. Dennison, JR, Jodie Gillespie, Joshua Hodges, RC Hoffmann, J Abbott, Alan W. Hunt and Randy Spalding, "Radiation Induced Conductivity of Highly-Insulating Spacecraft Materials," in *Application of Accelerators in Research and Industry*, American Institute of Physics Conference Proceedings Series, Vol. 1099, ed. Floyd D. McDaniel and Barney L. Doyle,(American Institute of Physics, Melveille, NY, 2009), pp. 203-208.